

Molecular Physics

An International Journal at the Interface Between Chemistry and Physics

ISSN: 0026-8976 (Print) 1362-3028 (Online) Journal homepage: <https://www.tandfonline.com/loi/tmph20>

Quadrupole relaxation enhancement and polarisation transfer in DMSO solution of $[\text{Bi}(\text{NO}_3)_3(\text{H}_2\text{O})_3]^*18\text{-crown-6}$ in solid state

Danuta Kruk, Elzbieta Masiewicz, Evrim Umut, Martin Schögl, Roland Fischer & Hermann Scharfetter

To cite this article: Danuta Kruk, Elzbieta Masiewicz, Evrim Umut, Martin Schögl, Roland Fischer & Hermann Scharfetter (2019) Quadrupole relaxation enhancement and polarisation transfer in DMSO solution of $[\text{Bi}(\text{NO}_3)_3(\text{H}_2\text{O})_3]^*18\text{-crown-6}$ in solid state, Molecular Physics, 117:7-8, 944-951, DOI: [10.1080/00268976.2018.1552798](https://doi.org/10.1080/00268976.2018.1552798)

To link to this article: <https://doi.org/10.1080/00268976.2018.1552798>



© 2018 The Author(s). Published by Informa UK Limited, trading as Taylor & Francis Group



Published online: 11 Dec 2018.



Submit your article to this journal [↗](#)



Article views: 482



View related articles [↗](#)



View Crossmark data [↗](#)



Citing articles: 1 View citing articles [↗](#)

Quadrupole relaxation enhancement and polarisation transfer in DMSO solution of $[\text{Bi}(\text{NO}_3)_3(\text{H}_2\text{O})_3] \cdot 18\text{-crown-6}$ in solid state

Danuta Kruk ^a, Elzbieta Masiewicz^a, Evrim Umut^a, Martin Schlögl^b, Roland Fischer^b and Hermann Scharfetter^c

^aFaculty of Mathematics and Computer Science, University of Warmia and Mazury in Olsztyn, Olsztyn, Poland; ^bInstitute of Inorganic Chemistry, Graz University of Technology, Graz, Austria; ^cInstitute of Medical Engineering, Graz University of Technology, Graz, Austria

ABSTRACT

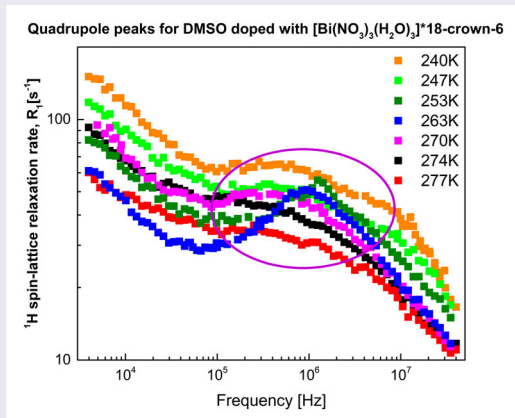
¹H spin-lattice relaxation studies have been performed for pure $[\text{Bi}(\text{NO}_3)_3(\text{H}_2\text{O})_3] \cdot 18\text{-crown-6}$ in powder and its solution in dimethyl sulfoxide (DMSO). The experiments have been carried out in the frequency range of 10 kHz–30 MHz and the temperature range of 240–277 K; at 277 K the solution is already frozen. The ¹H relaxation of pure $[\text{Bi}(\text{NO}_3)_3(\text{H}_2\text{O})_3] \cdot 18\text{-crown-6}$ has been interpreted in terms of three dynamical processes. Quadrupole Relaxation Enhancement effects have been observed in the frozen DMSO solution of $[\text{Bi}(\text{NO}_3)_3(\text{H}_2\text{O})_3] \cdot 18\text{-crown-6}$. The specific mechanisms of the ¹H spin-lattice relaxation enhancement have been discussed distinguishing between effects caused by time independent (residual) and fluctuating ¹H–²⁰⁹Bi dipole-dipole interactions.

ARTICLE HISTORY

Received 17 July 2018
Accepted 6 November 2018

KEYWORDS



NMR; relaxation; quadrupole peaks; polarization transfer



Introduction

Nuclear Magnetic Resonance (NMR) relaxometry is one of the most frequently used methods of studying dynamical processes in condensed matter. As a result of a broad frequency (magnetic field) range covered in NMR relaxometry, one can probe in a single experiment several dynamical processes of the time scale from ms to ns [1–3]. In this work NMR relaxometry studies of pure $[\text{Bi}(\text{NO}_3)_3(\text{H}_2\text{O})_3] \cdot 18\text{-crown-6}$ in powder and of its frozen solution in dimethyl sulfoxide (DMSO) are presented. The purpose of the studies is related to the concept of exploiting Quadrupole Relaxation Enhancement (QRE) [4–13] effects as a possible contrast mechanism for Magnetic Resonance Imaging (MRI) [14,15].

QRE is a quantum-mechanical phenomenon including at least one nucleus of spin quantum number $S \geq 1$, possessing a quadrupole moment (and thus referred to as a quadrupole nucleus) and a nucleus of spin $I = 1/2$ (for instance ¹H) mutually coupled by a dipole–dipole interaction. When the principal axis system of the electric field gradient tensor at the position of the quadrupole nucleus does not change its orientation with respect to the direction of the external magnetic field (this takes place in solids or solutions in which the object carrying the quadrupole nucleus undergoes slow rotational dynamics), the energy level structure of the quadrupole nucleus stems from a superposition of its quadrupole and Zeeman interactions. In consequence, there are magnetic

CONTACT Danuta Kruk  danuta.kruk@matman.uwm.edu.pl  Faculty of Mathematics and Computer Science, University of Warmia and Mazury in Olsztyn, Słoneczna 54, Olsztyn PL-10710, Poland

© 2018 The Author(s). Published by Informa UK Limited, trading as Taylor & Francis Group
This is an Open Access article distributed under the terms of the Creative Commons Attribution-NonCommercial-NoDerivatives License (<http://creativecommons.org/licenses/by-nc-nd/4.0/>), which permits non-commercial re-use, distribution, and reproduction in any medium, provided the original work is properly cited, and is not altered, transformed, or built upon in any way.

fields at which the transition energy of the nucleus of spin 1/2 (the resonance frequency) matches one of the transitions of the quadrupole nucleus between its energy levels. At these magnetic fields the 1/2 spin (for instance ^1H) magnetisation can be ‘taken over’ by the quadrupole nucleus provided the participating spins are coupled by a dipole – dipole interaction. In case the dipole–dipole coupling does not fluctuate in time, the effect of losing the ^1H magnetisation is referred to as polarisation transfer [2,16–18]. Otherwise (for fluctuating dipole–dipole interactions) one talks about QRE. In practice, both effects are often referred to as QRE as a drop of the ^1H magnetisation can always be seen as a faster ^1H spin–lattice relaxation (although time independent interactions do not cause relaxation). Thus, independently of its specific mechanism, the loss of the ^1H magnetisation is often interpreted as a frequency specific increasing of the spin–lattice relaxation rate, while the relaxation maxima are called quadrupole peaks. Comparing QRE with Paramagnetic Relaxation Enhancement (PRE) [19–21] (exploited in MRI as a contrast mechanism), the most fundamental difference lies in the fact that PRE is present at an arbitrary frequency as it stems from the strong electron spin – proton spin dipole – dipole coupling, while QRE only appears at specific frequencies. In consequence, MRI contrast based on the QRE effect can be switched on and off in response to subtle changes of the electric field gradient in pathological tissues. The potential of QRE based contrast agents has been discussed in our recent papers [14,15]. ^{209}Bi has been selected as the quadrupole nucleus because of its large quadrupole moment that leads to QRE peaks in the vicinity of the magnetic fields (1.5 and 3 T) of commercial medical scanners, high spin and gyromagnetic factor as well as ‘rich chemistry’ that allows for tuning the NQR frequencies by different ligands. Despite the encouraging output of our studies [14,15,22], there is several factors that can obscure the QRE effects. One of them is the ^1H – ^1H relaxation contribution originating from interactions between the solvent molecules (DMSO in this case) and solvent and solute molecules (DMSO – $[\text{Bi}(\text{NO}_3)_3(\text{H}_2\text{O})_3]^*18\text{-crown-6}$ in this case). Using the example of ^1H relaxation processes in DMSO solution of $[\text{Bi}(\text{NO}_3)_3(\text{H}_2\text{O})_3]^*18\text{-crown-6}$, we aim to inquire into how the ^1H – ^1H relaxation channel can influence the discernibility of QRE effects to get better understanding of this disadvantageous effect. Independently of that, the second goal of this work is to illustrate the difference between polarisation transfer (associated with a time-independent dipole–dipole interaction) and QRE effects (associated with a fluctuating dipole–dipole interaction). This is important from the viewpoint of applying NMR relaxometry to investigate dynamics of solids as an

erroneous identification of the origin of the quadrupole peaks can lead to misinterpretations of the relaxation data in terms of the underlying dynamical processes (Table 1).

Theory

Dipole–dipole interactions are the dominating mechanism of ^1H relaxation and polarisation transfer. Figure 1(a–c) illustrates the difference between the ^1H relaxation enhancement and the polarisation transfer [2,16,23]. QRE is associated with a fluctuating ^1H -X (X denotes a quadrupole nucleus) dipole–dipole coupling. The correlation time characterising the fluctuations has to fulfil the condition: $\omega_{DD}\tau_c < 1$, where ω_{DD} denotes the amplitude of the ^1H -X dipole–dipole coupling in angular frequency units. To observe quadrupole peaks resulted from the QRE two more conditions have to be fulfilled. The first one yields: $\omega_{QRE}\tau_c \geq 1$, where ω_{QRE} is the frequency (in angular frequency units) at which one expects the QRE peak to appear (*i.e.* one of the transition frequencies of the quadrupole nucleus). The second condition requires that there is a quadrupolar coupling for which the orientation of the principal axes system is fixed with respect to the direction of the external magnetic field. This can be achieved in two ways: the molecule carrying the X nucleus undergoes a slow dynamics (is immobilised) or there is a residual quadrupole interaction (a non-zero effect of a long-time average) due to anisotropic motion (typical of solids). This situation is depicted in Figure 1(a). When $\omega_{DD}\tau_c < 1$, but the other two conditions are not fulfilled, there is a ^1H -X dipole–dipole contribution to the overall ^1H relaxation, but it does not exhibit quadrupole peaks – Figure 1(b). Eventually, when $\omega_{DD}\tau_c \gg 1$ as a result of slow dynamics or there is a residual ^1H -X dipole–dipole coupling, the ^1H relaxation maxima appear as a result of a polarisation transfer – Figure 1(c).

In the case of $[\text{Bi}(\text{NO}_3)_3(\text{H}_2\text{O})_3]^*18\text{-crown-6}$ molecules one should consider ^1H – ^1H , ^1H – ^{14}N and ^1H – ^{209}Bi dipolar couplings. Focusing on ^1H – ^1H dipole–dipole interactions and taking into account that relaxation experiments performed versus the magnetic field (resonance frequency) reflect motional processes on different timescales, one can express the corresponding spin–lattice relaxation contribution, $R_1^{HH}(\omega)$, as [24–28]:

$$R_1^{HH}(\omega) = \sum_n C_{DD,n} \left[\frac{\tau_{c,n}}{1 + (\omega\tau_{c,n})^2} + \frac{4\tau_{c,n}}{1 + (2\omega\tau_{c,n})^2} \right] \quad (1)$$

where $\tau_{c,n}$ denotes the correlation time of n -th dynamical process, while $C_{DD,n}$ is the corresponding dipolar relaxation constant. As far as the relaxation contribution originating from a dipole–dipole coupling between ^1H

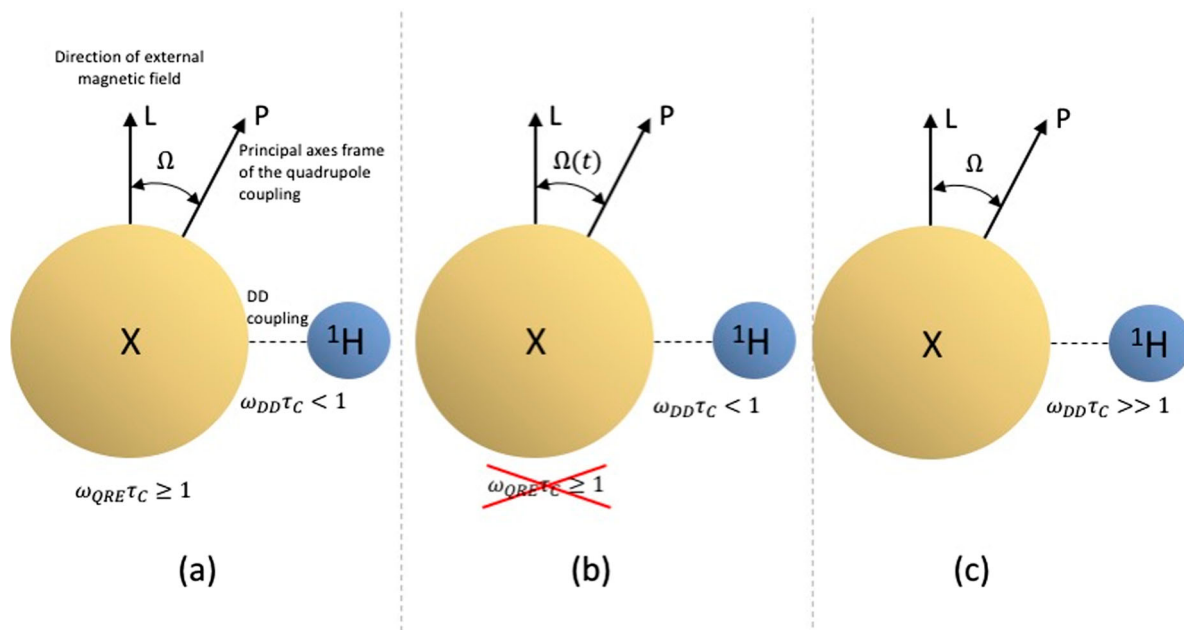


Figure 1. Schematic representation of QRE and polarisation transfer effects; X denotes a nucleus possessing quadrupole moment.

and a quadrupole nucleus is concerned, the theoretical description is much more complex and it depends on the time scale of the dynamics of the system [7,27,28]. For a time dependent ^1H -X (X denotes a quadrupole nucleus) dipole – dipole coupling the theory is based on the second-rank perturbation approach, *i.e.* Redfield relaxation theory [20] when the fluctuations of the orientation of the principal axis system of the electric field gradient with respect to the direction of the external magnetic field is very slow or very fast [2,9,23] and on the Stochastic Liouville Equation (SLE) for arbitrary motional conditions [7–9, 29–33]. For a time independent ^1H -X dipole-dipole coupling the polarisation transfer is described by time independent Liouville Equation [2,17,23]. The main concept of the theory of QRE is outlined in Appendix A.

Experimental details

$[\text{Bi}(\text{NO}_3)_3(\text{H}_2\text{O})_3] \cdot 18\text{-crown-6}$, as an example of BiX_3 -crown ether compounds, has a structure based on a pyramidal BiX_3 group with open faces weakly covered by crown. Bismuth is coordinated to three bidentate nitrates and to three water molecules, with the crown bonded to water by H-bonding but not interacting directly with bismuth [30]. The structure of $[\text{Bi}(\text{NO}_3)_3(\text{H}_2\text{O})_3] \cdot 18\text{-crown-6}$ is shown in Figure 2.

^1H spin–lattice relaxation experiments have been performed for $[\text{Bi}(\text{NO}_3)_3(\text{H}_2\text{O})_3] \cdot 18\text{-crown-6}$ in solid form (powder) and its solution in DMSO (25 mMol) by using a Stellar Spinmaster FFC relaxometer in the frequency range of 10 kHz–30 MHz (referring to ^1H). The experiments for solid $[\text{Bi}(\text{NO}_3)_3(\text{H}_2\text{O})_3] \cdot 18\text{-crown-6}$

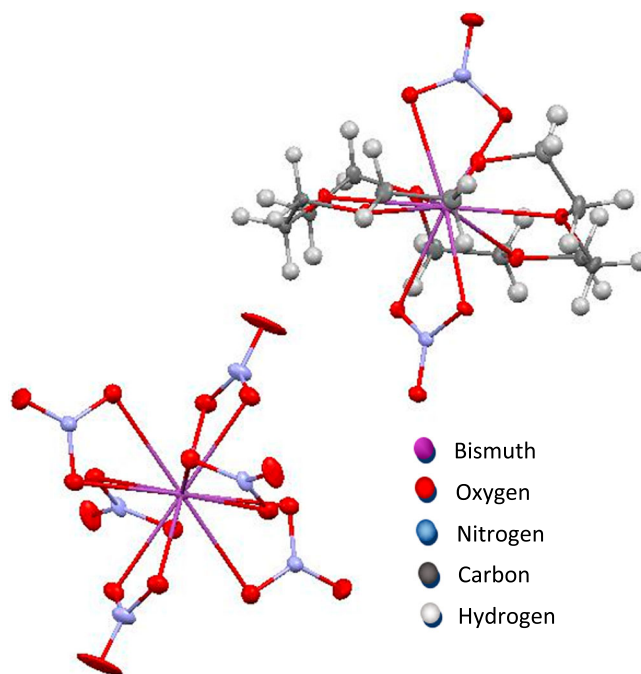


Figure 2. Structure of $[\text{Bi}(\text{NO}_3)_3(\text{H}_2\text{O})_3] \cdot 18\text{-crown-6}$.

and the solution have been performed in the temperature range of 240–277 K. One should stress that in this temperature range the solution is frozen. As a reference ^1H spin–lattice relaxation profiles have also been collected for pure DMSO at the corresponding temperatures. In all cases the relaxation process has turned out to be single exponential. Examples of ^1H magnetisation curves recorded versus time for selected frequencies are shown in Appendix B (Figure B1).

Results and discussion

The relaxation data for $[\text{Bi}(\text{NO}_3)_3(\text{H}_2\text{O})_3] \cdot 18\text{-crown-6}$ in powder are shown in Figure 3. The data have been interpreted in terms of three motional processes according to Equation (1). They are referred to as slow, intermediate and fast ones. The correlation time of the fast process is too short to lead to a visible relaxation dispersion. Therefore, it manifests itself as a frequency independent term, A . The slow and intermediate processes are represented by the correlation times $\tau_{c,s}$ and $\tau_{c,i}$, respectively, and the corresponding dipolar relaxation constants, $C_{DD,s}$ and $C_{DD,i}$. Thus, the fits have been performed with five adjustable parameters: $C_{DD,s}$, $\tau_{c,s}$, $C_{DD,i}$, $\tau_{c,i}$ and A . The dipolar relaxation constants have been kept temperature independent amounting to: $C_{DD,s} = 2.82 \cdot 10^9 \text{ Hz}^2$ and $C_{DD,i} = 1.41 \cdot 10^9 \text{ Hz}^2$. The decomposition of the overall relaxation data into contributions associated with the slow, intermediate and fast dynamical processes is shown in Figure 4, while in Figure 5 the obtained correlation times are plotted versus reciprocal temperature. They follow the Arrhenius law with very similar activation energies. The compound includes two proton pools: one formed by the crown protons and one formed by the water protons. The ratio between the number of protons belonging to these two pools yields 2/9. This implies that one can see both of them in the relaxation experiments. One can attribute the obtained correlation times to the dynamics of the proton pools: the slow process to crown and the intermediate process to water, although one cannot prove this assignment on the basis of the relaxation data. The frequency independent contribution, A , can represent fast internal dynamics of crown molecules. As far as the ^1H - ^{14}N and

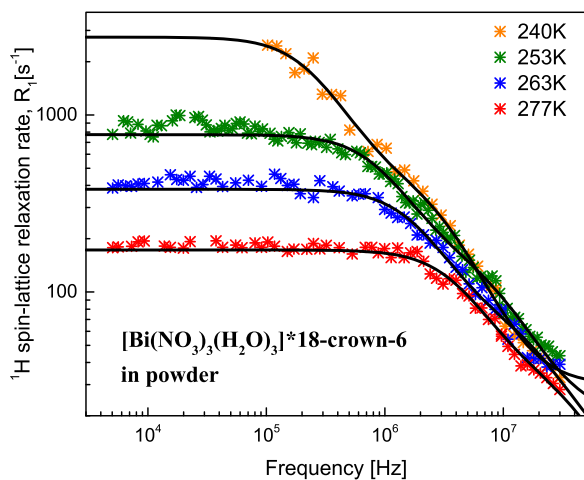


Figure 3. ^1H spin-lattice relaxation data for pure $[\text{Bi}(\text{NO}_3)_3(\text{H}_2\text{O})_3] \cdot 18\text{-crown-6}$ in powder at 240, 253, 263 and 277 K; solid lines – theoretical fits.

Table 1. Parameters obtained from the analysis of ^1H spin-lattice relaxation rate profiles for $[\text{Bi}(\text{NO}_3)_3(\text{H}_2\text{O})_3] \cdot 18\text{-crown-6}$ in powder; $C_{DD,s} = 2.82 \cdot 10^9 \text{ Hz}^2$, $C_{DD,i} = 1.41 \cdot 10^9 \text{ Hz}^2$.

$T[\text{K}]$	$\tau_{c,s}[\text{s}]$	$\tau_{c,i}[\text{s}]$	$A[\text{s}^{-1}]$	relative error [%]
240	$3.32 \cdot 10^{-7}$	$2.70 \cdot 10^{-8}$	30	6.1
253	$8.92 \cdot 10^{-8}$	$8.91 \cdot 10^{-9}$	20	11.5
263	$4.47 \cdot 10^{-8}$	$3.98 \cdot 10^{-9}$	9.2	17.6
277	$2.00 \cdot 10^{-8}$	$2.00 \cdot 10^{-9}$	3.6	10.2

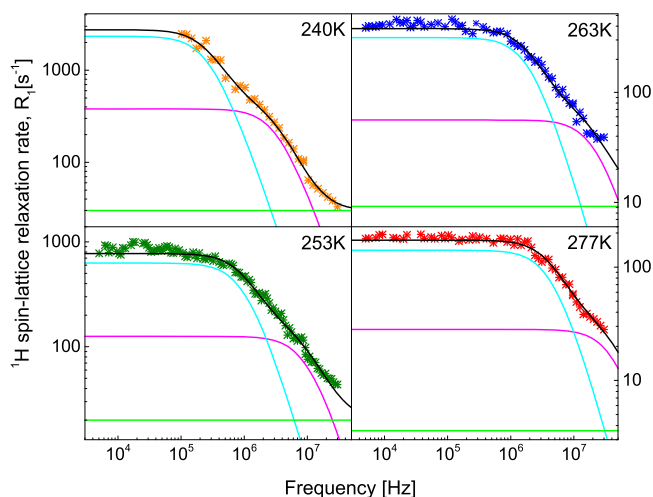


Figure 4. ^1H spin-lattice relaxation data for $[\text{Bi}(\text{NO}_3)_3(\text{H}_2\text{O})_3] \cdot 18\text{-crown-6}$ in powder; black lines – theoretical fits decomposed into relaxation contributions associated with the slow (light blue lines), intermediate (violet lines) and fast (light green lines) dynamical processes.

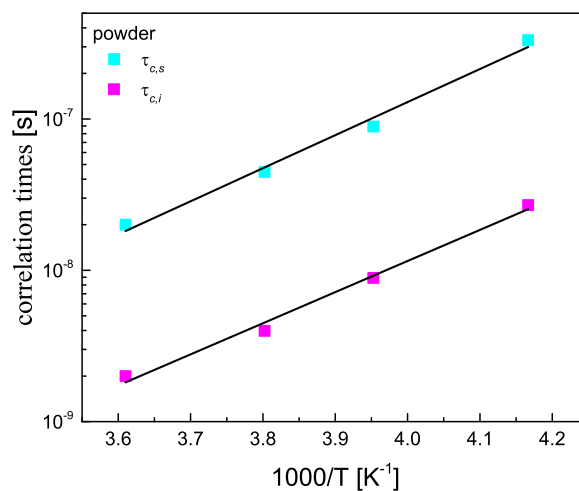


Figure 5. Correlation times (solid symbols) for $[\text{Bi}(\text{NO}_3)_3(\text{H}_2\text{O})_3] \cdot 18\text{-crown-6}$ in powder versus reciprocal temperature. Solid lines – linear fits according to the Arrhenius law: activation energy: 39.29 kJ/(mol*K) ($\tau_{c,s}$) and 41.75 kJ/(mol*K) ($\tau_{c,i}$).

^1H - ^{209}Bi relaxation contributions are concern, there is no indication that they considerably contribute to the ^1H relaxation in $[\text{Bi}(\text{NO}_3)_3(\text{H}_2\text{O})_3] \cdot 18\text{-crown-6}$ in powder.

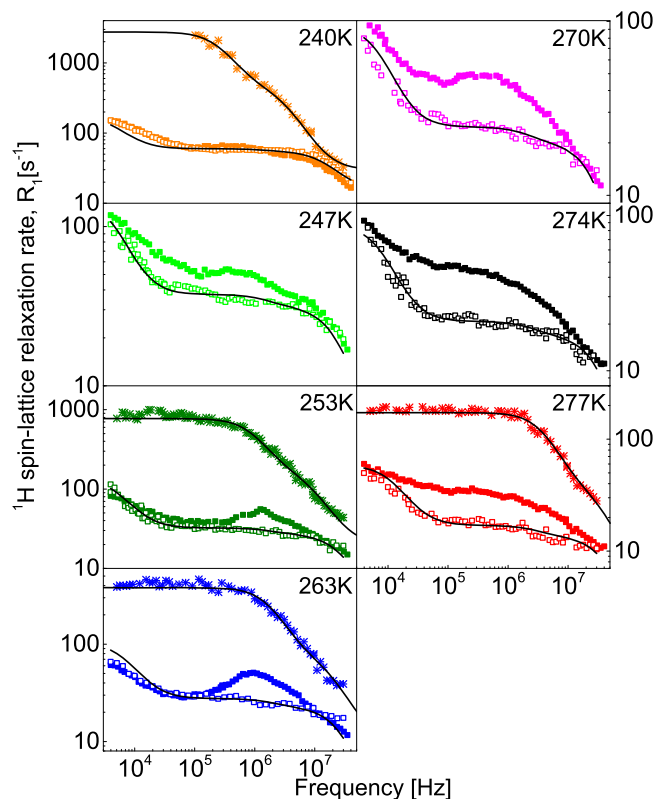


Figure 6. Comparison of ^1H spin-lattice relaxation data for $[\text{Bi}(\text{NO}_3)_3(\text{H}_2\text{O})_3]\cdot 18\text{-crown-6}$ in powder (stars), frozen solution of $[\text{Bi}(\text{NO}_3)_3(\text{H}_2\text{O})_3]\cdot 18\text{-crown-6}$ in DMSO (solid squares) and pure DMSO (open squares); solid lines – theoretical fits.

In the next step we have considered ^1H spin – lattice relaxation data for pure DMSO. The data are shown in Appendix B (Figure B2). They have also been analysed in terms of three motional processes referred to as slow, intermediate and fast ones. The fast dynamics can be associated with the methyl groups rotation in DMSO. As the molecule has a two-fold symmetry axis one can think about its reorientational jumps as a possible source of the slower dynamics. The complex dynamics of frozen DMSO is of interest by itself, but we shall not discuss this subject in this paper. The fits, decomposed into the individual contributions, are shown in Appendix B (Figure B2), which also contains the obtained parameters.

Now we turn attention to the relaxation data for DMSO solution of $[\text{Bi}(\text{NO}_3)_3(\text{H}_2\text{O})_3]\cdot 18\text{-crown-6}$. At this point it is important to stress that as the ratio between the number of protons of $[\text{Bi}(\text{NO}_3)_3(\text{H}_2\text{O})_3]\cdot 18\text{-crown-6}$ and of DMSO for 0.25 mMol concentration is below 1%, we observe in the experiment the relaxation process of the solvent (DMSO) molecules. The data for the solution are much different (for most of the temperatures) than for pure DMSO. In Figure 6 they are compared not only with themselves, but also with the data for

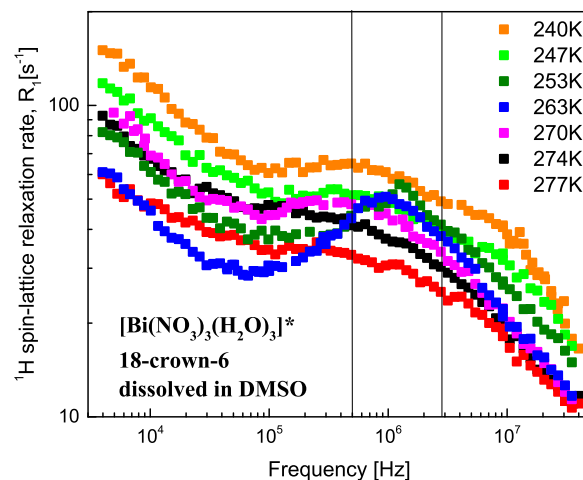


Figure 7. ^1H spin-lattice relaxation data for $[\text{Bi}(\text{NO}_3)_3(\text{H}_2\text{O})_3]\cdot 18\text{-crown-6}$ dissolved in DMSO (25mMol). Vertical lines indicate the frequency range in which the ^1H resonance frequency matches single-quantum transitions frequencies of ^{209}Bi for $a_Q = 14.9\text{ MHz}$ and $\eta = 0$.

$[\text{Bi}(\text{NO}_3)_3(\text{H}_2\text{O})_3]\cdot 18\text{-crown-6}$ in powder at 240, 253, 263 and 277 K.

Two main observations can be made looking at the comparison between the data for the solution and for the powder: although the relaxation is slower for the frozen solution that for the powder it shows a much more considerable dispersion at low frequencies, and (in contrary to $[\text{Bi}(\text{NO}_3)_3(\text{H}_2\text{O})_3]\cdot 18\text{-crown-6}$ in powder) QRE effects are observed. To follow changes in the QRE effects with temperature in Figure 7 the relaxation data for the DMSO solution of $[\text{Bi}(\text{NO}_3)_3(\text{H}_2\text{O})_3]\cdot 18\text{-crown-6}$ collected in the whole temperature range are presented. At this stage one should point out that taking into account the molecular structure, the gyromagnetic factors of ^{209}Bi and ^{14}N and their spins, one can estimate that the ^1H -X relaxation contribution is mainly associated with ^{209}Bi .

The comparison between the relaxation data for pure DMSO and the solution requires a more elaborated discussion. Let us begin with the lowest temperature of 240 K. At this temperature there is no much difference between the relaxation of pure DMSO and the DMSO solution (Figure 6). Thus one could conclude that the ^1H - ^{209}Bi relaxation contribution to the overall ^1H spin-lattice relaxation of the solution is of minor importance. This is a misleading statement. At the higher temperature, 247 K, dynamical processes in the system become faster and, in consequence, the ^1H - ^1H relaxation contribution at low and intermediate frequencies becomes smaller. In this way, the effect of ^1H - ^{209}Bi dipole-dipole interactions becomes visible. The more pronounced QRE at a higher temperature

indicates that this effect (at least its considerable part) should be attributed to a time independent (residual) ^1H - ^{209}Bi dipole–dipole coupling; thus one should rather talk about a polarisation transfer. Otherwise a faster dynamics would lead to even less visible QRE [27,28] as the product $\omega_{\text{QRE}}\tau_c$ would decrease. One can consider the ^1H - ^{209}Bi dipole – dipole interaction as a superposition of a time independent part causing the polarisation transfer and a time dependent part fluctuating around this averaged value and causing ^1H relaxation. The concept of a polarisation transfer caused by a residual ^1H - ^{209}Bi dipole – dipole coupling is confirmed by the data at 253 and 263 K – the polarisation transfer peak becomes progressively more visible due to decreasing of the ^1H - ^1H relaxation contribution; they do not disappear with faster dynamics. Nevertheless, one can expect that with increasing temperature the amplitude of a residual spin interaction becomes lower and/or as the time scale of its fluctuations becomes shorter, the interaction cannot be anymore treated as time independent (the fluctuations are not anymore much slower than the relaxation process). These effects are seen at the higher temperatures: 270, 274 and 277 K. The ^1H - ^1H relaxation contribution becomes smaller revealing more of the ^1H - ^{209}Bi term that itself becomes progressively broader, eventually losing its peak (277 K). This can be understood as a result of a decreasing magnitude of the residual ^1H - ^{209}Bi dipole – dipole coupling. It might be of interest to attempt to determine the ^{209}Bi quadrupole parameters for $[\text{Bi}(\text{NO}_3)_3(\text{H}_2\text{O})_3]^*18$ -crown-6. This has turned out to be impossible by means of Nuclear Quadrupole Resonance (NQR), probably due to too fast spin–spin relaxation of ^{209}Bi . Therefore, the ^1H spin–lattice relaxation data for the DMSO solution of $[\text{Bi}(\text{NO}_3)_3(\text{H}_2\text{O})_3]^*18$ -crown-6 are the only source of information on this subject. As the quadrupole peak is very broad with no visible splitting, one can expect that the asymmetry parameter η [15,26,27] is small. Setting $\eta = 0$ we have diagonalised the total Hamiltonian of the ^{209}Bi spin ($S = 9/2$) composed of its Zeeman and quadrupole interaction in order to obtain the energy level structure of ^{209}Bi as a function of the magnetic field with the amplitude of the quadrupole coupling constant, a_Q [15,26,27] as a parameter. The procedure of determining the energy level structure has been described in [15]. Figure 7 shows the frequency range in which the ^1H resonance frequency matches several ^{209}Bi spin transitions for $a_Q = 14.9$ MHz and $\eta = 0$. The range is in the area of the broad quadrupole peak.

Summarising, the presented results are an example of simultaneous effects of ^1H polarisation transfer and relaxation enhancement. They illustrate a complex interplay between spin interactions in systems containing quadrupole nuclei.

Conclusions

Motivated by the perspective of exploiting QRE effects as a novel contrast mechanism for MRI, ^1H spin–lattice relaxation experiments for $[\text{Bi}(\text{NO}_3)_3(\text{H}_2\text{O})_3]^*18$ -crown-6 and its frozen solution in DMSO. Due to slow dynamics combined with strong anisotropic interactions, typical of solids, in the frozen solution a combination of a polarisation transfer (caused by a time independent ^1H - ^{209}Bi dipole – dipole coupling) and ^1H spin–lattice relaxation enhancement (caused by a fluctuating part of the ^1H - ^{209}Bi dipole – dipole interaction). The temperature changes of the relaxation dispersion profiles have been explained in terms of the two mechanisms.

Acknowledgement

This project has received funding from the European Union's Horizon 2020 research and innovation programme under grant agreement No 665172. The authors also acknowledge the COST Action CA15209, supported by COST (European Cooperation in Science and Technology) which stimulated relevant personal communications with several NMR relaxometry experts.

Disclosure statement

No potential conflict of interest was reported by the authors.

Funding

This project has received funding from the European Union's Horizon 2020 research and innovation programme under grant agreement No 665172. The authors also acknowledge the COST Action CA15209, supported by COST (European Cooperation in Science and Technology) which stimulated relevant personal communications with several NMR relaxometry experts.

ORCID

Danuta Kruk  <http://orcid.org/0000-0003-3083-9395>

References

- [1] R. Kimmich and E. Anoardo, *Prog. Nucl. Magn. Reson. Spectrosc.* **44**, 257 (2004).
- [2] F. Fujara, D. Kruk, and A.F. Privalov, *Prog. Nucl. Magn. Reson. Spectrosc.* **82**, 39 (2014).
- [3] R. Meier, D. Kruk, and E.A. Rössler, *ChemPhysChem.* **14**, 3071 (2013).
- [4] F. Winter and R. Kimmich, *Mol. Phys.* **45**, 33 (1982).
- [5] E. Anoardo and D.J. Pusiolo, *Phys. Rev. Lett.* **76**, 3983 (1996).
- [6] P.-O. Westlund, *Mol. Phys.* **107**, 2141 (2009).
- [7] E.P. Sunde and B. Halle, *J. Magn. Reson.* **203**, 257 (2010).
- [8] P.-O. Westlund, *Phys. Chem. Chem. Phys.* **12**, 3136 (2010).
- [9] D. Kruk, A. Kubica, W. Masierak, A.F. Privalov, M. Wojciechowski, and W. Medycki, *Solid State Nucl. Magn. Reson.* **40**, 114 (2011).

- [10] D.J. Lurie, S. Aime, S. Baroni, N.A. Booth, L.M. Broche, C.-H. Choi, G.R. Davies, S. Ismail, D. Ó hÓgáin, and K.J. Pine, *Comptes Rendus Phys.* **11**, 136 (2010).
- [11] L.M. Broche, S.R. Ismail, N.A. Booth, and D.J. Lurie, *Magn. Reson. Med.* **67**, 1453 (2012).
- [12] W. Masierak, M. Florek-Wojciechowska, I. Oglodek, R. Jakubas, A.F. Privalov, B. Kresse, F. Fujara, and D. Kruk, *J. Chem. Phys.* **142**, 204503 (2015).
- [13] M. Florek-Wojciechowska, M. Wojciechowski, R. Jakubas, S. Brym, and D. Kruk, *J. Chem. Phys.* **19**, 11197 (2016).
- [14] C. Gösweiner, P. Lantto, R. Fischer, C. Sampl, E. Umut, P.-O. Westlund, D. Kruk, M. Bödenler, S. Spirk, A. Petrovič, and H. Scharfetter, *Phys. Rev. X* **8**, 021076 (2018).
- [15] D. Kruk, E. Umut, E. Masiewicz, C. Sampl, R. Fischer, S. Spirk, C. Gösweiner, and H. Scharfetter, *Phys. Chem. Chem. Phys.* **20**, 12710 (2018).
- [16] D. Kruk, A. Privalov, W. Medycki, C. Uniszkievicz, W. Masierak, and R. Jakubas, *Annu. Rep. NMR Spectrosc.* **76**, 67 (2012).
- [17] D. Kruk, J. Altmann, F. Fujara, A. Gadke, M. Nolte, and A.F. Privalov, *J. Phys. Condens. Matter.* **17**, 519 (2005).
- [18] M. Nolte, A. Privalov, J. Altmann, V. Anferov, and F. Fujara, *J. Phys. D Appl. Phys.* **35**, 939 (2002).
- [19] S. Aime, M. Botta, L. Frullano, S. Geninatti Crich, G. Giovenzana, R. Pagliarin, G. Palmisano, F. Riccardi Sirtori, and M. Sisti, *J. Med. Chem.* **43**, 4017 (2000).
- [20] P. Caravan, J.J. Ellison, T.J. McMurry, and R.B. Lauffer, *Chem. Rev.* **99**, 2293 (1999).
- [21] C.F.G.C. Geraldes, and S. Lauren, *Contrast Media Mol. Imaging.* **4**, 1 (2009).
- [22] M. Bödenler, M. Basini, M.F. Casula, E. Umut, C. Gösweiner, A. Petrovic, D. Kruk, and H. Scharfetter, *J. Magn. Reson.* **290**, 68 (2018).
- [23] D. Kruk, F. Fujara, P. Gumann, W. Medycki, A.F. Privalov, and C. Tacke, *Solid State Nucl. Magn. Reson.* **35**, 152 (2009).
- [24] I. Solomon and N. Bloembergen, *J. Chem. Phys.* **25**, 261 (1956).
- [25] N. Bloembergen and L.O. Morgan, *J. Chem. Phys.* **34**, 842 (1961).
- [26] A. Abragam, *The Principles of Nuclear Magnetism* (Oxford University Press, Oxford, 1961).
- [27] C. Slichter, *Principles of Magnetic Resonance* (Springer-Verlag, Berlin, 1990).
- [28] A. Redfield, in *Encyclopedia of Nuclear Magnetic Resonance*, edited by D. Grant and R. Harris (Wiley & Sons. Ltd., Chichester, 1996), pp. 4085–4092.
- [29] P.-O. Westlund, in *Dynamics of Solutions and Fluid Mixtures by NMR*, edited J. J. Delpuech (Wiley & Sons. Ltd., Chichester, 1995).
- [30] D.J. Schneider and J.H. Freed, *Adv. Chem. Phys.* **73**, 387 (1989).
- [31] T. Nilsson and J. Kowalewski, *J. Magn. Reson.* **146**, 345 (2000).
- [32] N. Benetis, J. Kowalewski, L. Nordenskiöld, H. Wennerström, and P.-O. Westlund, *Mol. Phys.* **48**, 329 (1983).
- [33] T. Nilsson, J. Svoboda, P.-O. Westlund, and J. Kowalewski, *J. Chem. Phys.* **109**, 6364 (1998).

Appendices

Appendix A

In the case of hetero-nuclear dipole-dipole interactions between spins I and S , the spin-lattice relaxation rate of spin I , $R_{1,I}$, is given as [26–28]:

$$R_{1,I} = \frac{2}{15} \left(\frac{\mu_0}{4\pi} \frac{\gamma_I \gamma_S \hbar}{r^3} \right)^2 S(S+1) \left[\frac{\tau_c}{1 + (\omega_I - \omega_S)^2 \tau_c^2} \right. \\ \left. \times + \frac{3\tau_c}{1 + \omega_I^2 \tau_c^2} + \frac{6\tau_c}{1 + (\omega_I + \omega_S)^2 \tau_c^2} \right] \quad (\text{A1})$$

where ω_I and ω_S denote the resonance frequency of spin I and spin S , respectively. This expression is valid as long as the energy level structure of spin S is determined entirely by its Zeeman interaction. In the presence of a quadrupole coupling which does not fluctuate with respect to the direction of the external magnetic field, Equation (A1) takes a more general form [9,23]:

$$R_{1,I} = \frac{2}{15} \left(\frac{\mu_0}{4\pi} \frac{\gamma_I \gamma_S \hbar}{r^3} \right)^2 S(S+1) \\ \times [s_{1,1}(\omega_I) + 3s_{0,0}(\omega_I) + 6s_{-1,1}(\omega_I)] \quad (\text{A2})$$

The quantities $s_{m,m}$ are referred to as generalised spectral densities. They can be obtained as a matrix product:

$$s_{m,m} = \text{Re}\{[S_m]^+ [M] [S_m]\} \quad (\text{A3})$$

The matrix $[M]$ is of the dimension of $(2S+1)^2$. In the simplest case, when the relaxation of the spin S caused by fluctuations of the electric field gradient at its position is negligible, the matrix is diagonal. It includes on the diagonal transition frequencies of the spin S between its energy levels (now determined by a superposition of the Zeeman and quadrupole couplings), ω_I and τ_c . The vector $[S_m]$ includes a series of coefficients representing S_m operators in the basis constructed from pairs of the eigenvectors of the Hamiltonian including the Zeeman and quadrupole couplings of the spin S ; ‘+’ denotes matrix transposition.

Appendix B

Examples of ^1H magnetisation curves:

^1H spin-lattice relaxation data for DMSO and their analysis:

Table B1. Parameters obtained from the analysis of ^1H spin-lattice relaxation rate profiles for DMSO; $C_{DD,S} = 1.29 \times 10^6$ [Hz 2], $C_{DD,i} = 2.82 \times 10^7$ [Hz 2], $C_{DD,f} = 1.43 \times 10^9$ [Hz 2].

T [K]	$\tau_{c,S}$ [s]	$\tau_{c,i}$ [s]	$\tau_{c,f}$ [s]	Average relative error [%]	maximum relative error [%]
240	1.84×10^{-5}	5.14×10^{-8}	5.42×10^{-9}	9.8	37.9
247	1.72×10^{-5}	4.94×10^{-8}	3.54×10^{-9}	7.3	23.7
253	1.68×10^{-5}	4.28×10^{-8}	3.26×10^{-9}	6.5	25.8
263	1.18×10^{-5}	4.08×10^{-8}	3.06×10^{-9}	8.1	23.1
270	1.07×10^{-5}	3.78×10^{-8}	2.71×10^{-9}	6.6	20.1
274	1.02×10^{-5}	3.18×10^{-8}	2.28×10^{-9}	6.1	18.5
277	6.46×10^{-6}	2.71×10^{-8}	1.84×10^{-9}	7.9	18.7

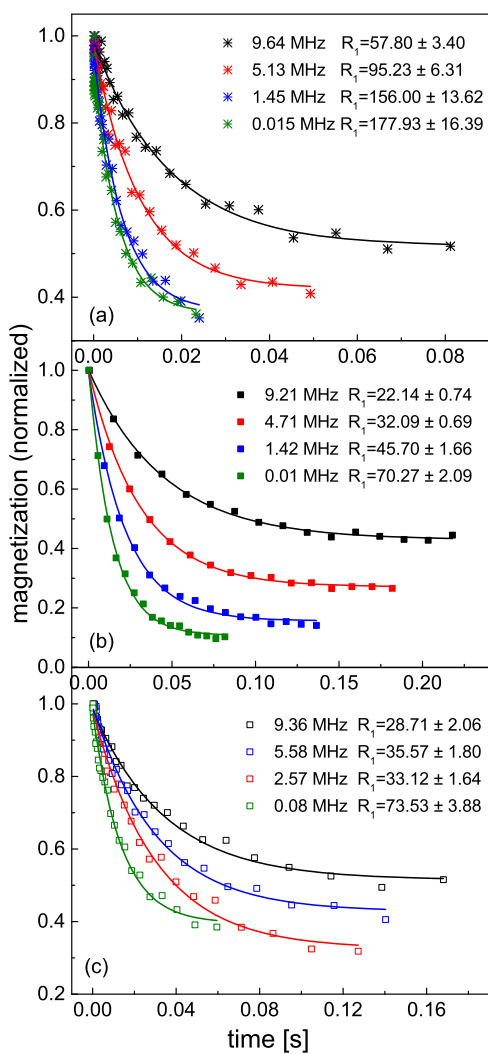


Figure B1. ^1H magnetisation versus time for: (a) solid $[\text{Bi}(\text{NO}_3)_3(\text{H}_2\text{O})_3] \cdot 18\text{-crown-6}$ at 277 K, (b) $[\text{Bi}(\text{NO}_3)_3(\text{H}_2\text{O})_3] \cdot 18\text{-crown-6}$ dissolved in DMSO at 277 K and (c) pure DMSO at 247 K. Solid lines show monoexponential fits.

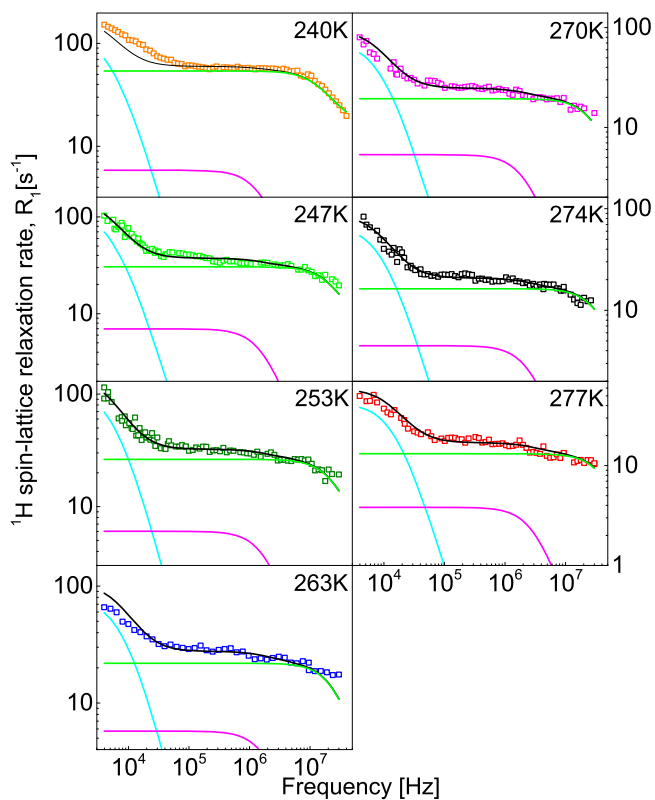


Figure B2. ^1H spin-lattice relaxation data for pure DMSO; black lines – theoretical fits decomposed into relaxation contributions associated with the slow (light blue lines), intermediate (violet lines) and fast (light green lines) dynamical processes.